Journal of Sound and Vibration 377 (2016) 243–263

Contents lists available at ScienceDirect

Journal of Sound and Vibration

journal homepage: www.elsevier.com/locate/jsvi

Correlation between quasi-static and dynamic experiments for a practical torsional device with multiple discontinuous nonlinearities

Michael D. Krak, Rajendra Singh*

Acoustics and Dynamics Laboratory, NSF Smart Vehicle Concepts Center, Department of Mechanical and Aerospace Engineering, The Ohio State University, Columbus, OH 43210, USA

ARTICLE INFO

Article history:
Received 12 November 2015
Received in revised form
25 April 2016
Accepted 1 May 2016
Handling Editor: L.N. Virgin
Available online 17 May 2016

Keywords:
Nonlinear isolators
Damping estimation
Energy dissipation mechanisms
Experimental methods
Nonlinear dynamics

ABSTRACT

Vehicle clutch dampers belong to a family of torsional devices or isolators that contain multi-staged torsional springs, pre-load features, clearances, and multi-staged dry friction elements. Estimation of elastic and dissipative parameters is usually carried out under quasi-static loading and then these static parameters are often assumed when predicting dynamic responses. For the purpose of comparison, this article proposes a new time domain parameter estimation method under dynamic, transient loading conditions. The proposed method assumes a priori knowledge of few nonlinear features based on the design and quasi-static characterization. Angular motion measurements from a component-level laboratory experiment under dynamic loading are utilized. Elastic parameters are first estimated through an instantaneous stochastic linearization technique. A model-based approach and energy balance principle are employed to estimate a combination of viscous and Coulomb damping parameters for seven local (stage-dependent) and global damping formulations for a practical device. The proposed method is validated by comparing time domain predictions from nonlinear models to dynamic measurements. Nonlinear models that utilize the proposed damping formulations are found to be superior to those that solely rely on parameters from a quasi-static experiment.

1. Introduction

There is an extensive body of literature on the estimation of system parameters [1–9]; see Ref. [1] for a thorough review of prior work as well as a list of over 300 papers. For the purpose of tractability, many researchers assume that nonlinear features or functions are well characterized (or known) before attempting parameter extraction [1]. Alternatively, the "black box" modeling method is used when the underlying physics of a device is truly unknown though ambiguous results may be found [1]. Overall, many of the estimation methods rely on steady-state excitation and assume smooth (differentiable) and/or weak nonlinearities [1]. Prior work [2–8] has often utilized measurements from well-controlled, laboratory or scientific experiments. These experiments [2–8] are intentionally designed to isolate a singular feature of interest, say a spring or dissipative element, and accommodate the necessary instrumentation. Although such methods and experiments are useful

* Corresponding author. Tel.: +1 614 292 9044.
E-mail address: singh.3@osu.edu (R. Singh).

http://dx.doi.org/10.1016/j.jsv.2016.05.003
0022-460X/

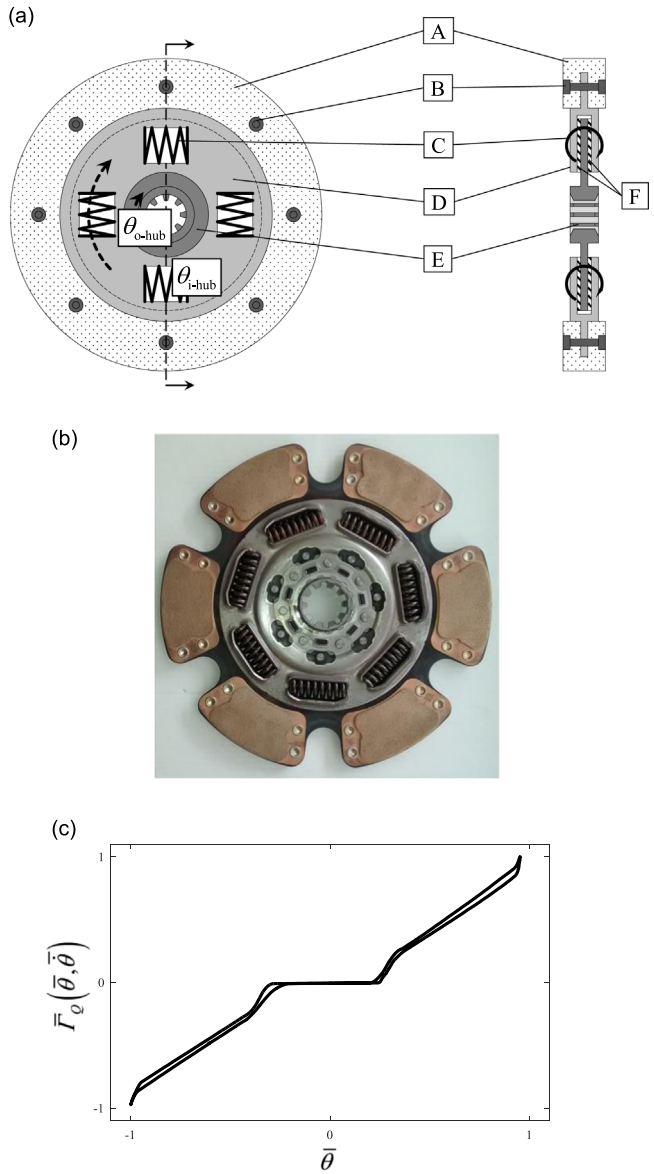

Fig. 1. Illustration of a multi-staged vehicle clutch damper: (a) schematic with parts labeled, (b) photograph of typical production component, and (c) measured (normalized) quasi-static performact curve where $\bar{\Gamma}_Q$ is the normalized torque transmitted through the device, $\bar{\theta}$ is the normalized relative angular displacment ($\theta = \theta_{o-\text{hub}} - \theta_{i-\text{hub}}$), and $\dot{\bar{\theta}}$ is the normalized relative angular velocity. Key for (a): A – flywheel and pressure plate interface; B – rivet; C – multi-staged coil spring; D – outer hub (angular displacement $\theta_{o-\text{hub}}$); E – inner hub (angular displacement $\theta_{i-\text{hub}}$); and F – multi-staged Coulomb friction element.

for understanding particular nonlinear features, their extension to practical devices [9–21] is severely limited by a lack of controllability found in many applications (say due to variability in manufacturing, assembly, or operating environment). This problem is particularly acute when practical components contain multiple (and yet unknown) discontinuous nonlinearities.

Most real-life components, including nonlinear devices used for vibration isolation [10], are subjected to a wide range of mean operating points and dynamic excitation due to intentional product functions. Even if these devices could be disassembled into separate nonlinear features for individual study, in situ interaction between the built-in features would be lost, and the estimation process would become incredibly complex. It is thus desirable to estimate parameters at the component-level. Nevertheless, this approach has its own unique challenges, such as laboratory space for large-scale experiments, selection of actuators than can provide in situ loading, and location and selection of instrumentation. Accordingly, the primary goal of this article is to propose a time domain method for estimating stiffness and damping properties of a nonlinear torsional isolation device (vehicle clutch damper) that is illustrated in Fig. 1a to b (and further described in Section 2). It has multiple discontinuous nonlinearities (as shown in Fig. 1c) and is often subject to dynamic,

transient loading over a large range of torques and angular displacements. The methods proposed in this article should benefit noise and vibration engineers and developers of nonlinear simulation codes while contributing to the scientific literature on non-smooth dynamic systems.

2. Example case and literature review

A typical vehicle clutch damper [11–21] primarily serves to transmit a mean torque while attenuating torque pulsations between an engine and transmission [11]. It is intentionally designed to contain multi-staged torsional springs, pre-load features, clearances, and multi-staged dry friction elements [11–21]. Furthermore, clutch dampers are often asymmetric; the drive side (positive relative angular displacement) of the device differs from its coast side (negative relative angular displacement) [11,12]. The typical torque range usually spans from near zero (under idling conditions) to as high as 1000–2000 N m (under driving conditions); to accommodate this, the ratio of torsional stiffness between adjacent stages may be as high as 100 [20,21]. It is common in high-load ground vehicles for two devices to be installed in a parallel configuration [21]; this introduces further complexity, such as indexing error and non-identical features. In practice, a clutch damper can be critical to controlling vibro-impact and impulsive loading phenomena in transmissions [14,15,19,20] and resonance growth during engine start-up [16]. Design and dynamic analysis of such a device could be facilitated by suitable nonlinear simulation tools.

A literature review of clutch dampers [11–21] shows that characterization is usually conducted at the component-level on a commercial test rig [22,23] under quasi-static loading conditions only. An example performance curve of a production clutch camper is shown in Fig. 1c where Γ_Q is the torque transmission and θ is the relative angular displacement. It is described by a multi-staged torsional spring in parallel with a multi-staged Coulomb friction element; elastic and dissipative parameters are then estimated from physical domain representations of torque transmission. Prior analysts [12,14–21] have assumed these static parameters when simulating dynamic responses of both the device itself and powertrain systems. Further, many models [12,14–16,21] include a parallel linear torsional viscous damper and assume damping values (or from a modal experiment) to improve agreement with measurement. This damping scheme relies on frequency domain methods

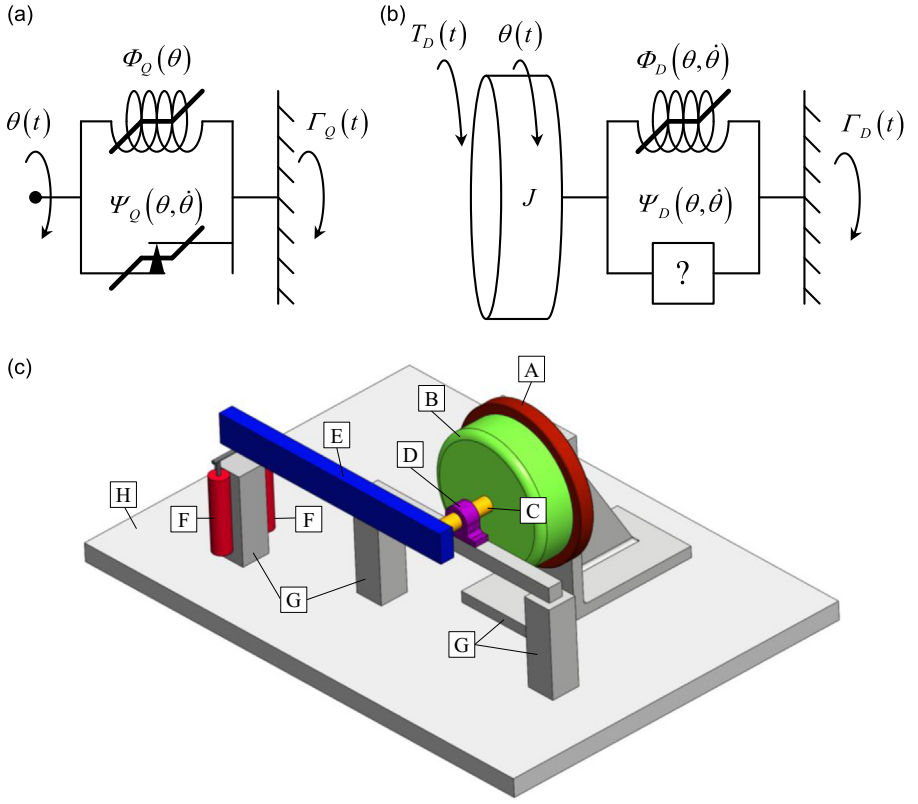

Fig. 2. Quasi-static and dynamic experiments for a vehicle clutch damper: (a) conceptual illustration for quasi-static loading (denoted X-Q); (b) conceptual and (c) physical illustrations for dynamic loading (denoted X-D) where θ is angular displacement, $\dot{\theta}$ is angular velocity, Φ is the elastic torque transmission, Ψ is the dissipative torque transmission, Γ is the total torque transmission ($\Gamma=\Psi+\Phi$), T is external torque, and J is torsional inertia. Key for (c): A – flywheel (ground); B – clutch assembly (houses one clutch damper); C – shaft; D – bearing; E – torsion arm; F – pneumatic actuators; G – structural supports (ground); and H – bed plate (ground).

and assumes that the operating range of the device lies within a single-stage. Thus, it is questionable to apply it to a transient nonlinear response in which the mean operating point varies significantly, spanning multiple stages rapidly (e.g. vehicle clunk phenomenon [14,19,20,24]). In addition, this parameter is sometimes extracted from a system-level measurement, such as provided by Biermann et al. [19] and Menday et al. [20]. While such experiments are valuable to understanding the role of clutch dampers within the context of a powertrain, they do not provide any physical insight at the component-level. To overcome this hurdle, Krak et al. [21] proposed a step-response type experiment, which is a simplified version of prior experiments [19,20,24]. Overall, there is clearly a void in the literature concerning the parameter estimation for vehicle clutch dampers (and similar devices) under dynamic, transient loading. The method proposed in this article will attempt to address this particular need; thus, both quasi-static and dynamic experiments are utilized and compared. Issues related to the mean shaft speed (such as the drag torque) are beyond the scope of this article.

3. Analytical formulation of problem

Consider a torsional device that contains multiple discontinuous nonlinear features, including multi-staged stiffness and dissipative elements. For practical reasons, manufacturers characterize such devices under quasi-static loading conditions only (relatively low angular velocity, denoted by subscript Q and conceptually illustrated in Fig. 2a). The governing equation of the device is the following where θ is the relative angular displacement, $T_Q(t)$ is external torque, J_ε is the associated torsional inertia ($J_\varepsilon \approx 0$), and $\Gamma_Q(\theta,\dot{\theta})$ is the torque transmitted through the device

$$J_\varepsilon \ddot{\theta} + \Gamma_Q(\theta,\dot{\theta}) = T_Q(t) \tag{1}$$

See Appendix A for a complete list of symbols. The torque transmitted through the device can be described by the following function where $\Psi_Q(\theta,\dot{\theta})$ is the dissipative torque and $\Phi_Q(\theta)$ is the elastic torque

$$\Gamma_Q(\theta,\dot{\theta}) = \Psi_Q(\theta,\dot{\theta}) + \Phi_Q(\theta) \tag{2}$$

For the sake of illustration, a symmetric, dual-staged example case is illustrated in Fig. 3; stages are denoted by subscript Roman numerals I and II, torsional stiffness is denoted by k, and angular stage transitions are denoted by Θ. The ratio of k_{I} to k_{II} is critical for describing $\Phi_Q(\theta)$; for instance, consider the following cases: a backlash is defined by $k_{\mathrm{I}} \to 0$ (or $k_{\mathrm{I}} \ll k_{\mathrm{II}}$); a preload feature requires $k_{\mathrm{I}} \to \infty$ (or $k_{\mathrm{I}} \gg k_{\mathrm{II}}$); a stopper element is given by $k_{\mathrm{II}} \to \infty$ (or $k_{\mathrm{II}} \gg k_{\mathrm{I}}$); and the linear spring element only occurs when $k_{\mathrm{I}} = k_{\mathrm{II}}$. The path-dependent nature of $\Gamma_Q(\theta,\dot{\theta})$ is due to $\Psi_Q(\theta,\dot{\theta})$, which is assumed to be described by Coulomb friction elements only.

Such devices usually operate under dynamic and high speed loading conditions (relatively high angular velocity, denoted by subscript D conceptually illustrated in Fig. 2b). Torque transmission may now be described by the function

$$\Gamma_D(\theta,\dot{\theta}) = \Psi_D(\theta,\dot{\theta}) + \Phi_D(\theta,\dot{\theta}) \tag{3}$$

Unlike the quasi-static conditions, it is assumed that $\Phi_D(\theta,\dot{\theta})$ may depend on both θ and $\dot{\theta}$, and $\Psi_D(\theta,\dot{\theta})$ may be described by viscous damping and/or Coulomb friction elements. The governing equation of the device is described below where $T_D(t)$ is external torque and J is the associated torsional inertia ($J \neq 0$)

$$J\ddot{\theta} + \Gamma_D(\theta,\dot{\theta}) = T_D(t). \tag{4}$$

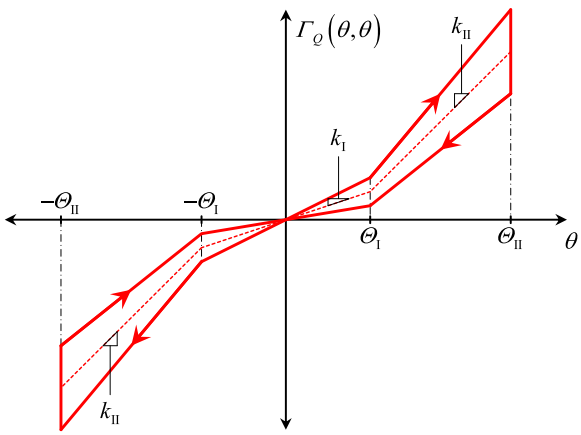

Fig. 3. Conceptual illustration of torque transmission through a symmetric, two-stage vehicle clutch damper under quasi-static loading conditions where $\Gamma_Q(\theta,\dot{\theta})$ is transmitted torque, θ is angular displacement, and $\dot{\theta}$ is angular velocity. Stages are denoted by subscripts I and II, torsional stiffness is denoted by k, and angular stage transitions are denoted by Θ. Key: (▬▶▬) – transmitted torque $\Gamma_Q(\theta,\dot{\theta})$; (▬ ▬) – elastic torque component $\Phi_Q(\theta)$; (– • –) – angular stage transition Θ; and (Δ) torsional stiffness k.

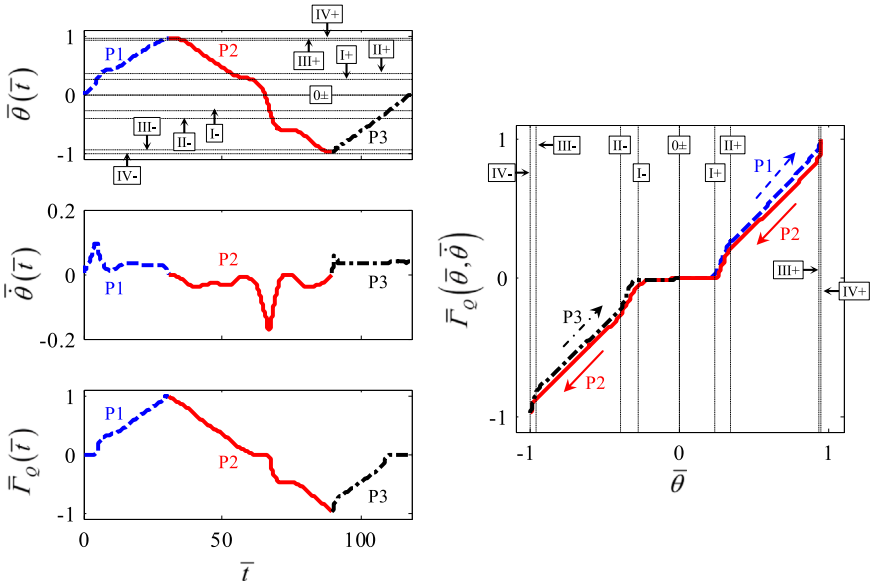

Fig. 4. Typical measurements in time and physical domains from quasi-static experiment X-Q where $\bar{\theta}$ is the normalized angular displacement, $\bar{\dot{\theta}}$ is the normalized angular velocity, $\bar{\Gamma}_Q$ is the normalized transmitted torque, and $\bar{t}$ is the normalized time. Key: (▬ ▬) – path P1; (▬) – path P2; (▪ ▪ ▪) – path P3; (– • –) – angular stage transitions $\Theta_{j\pm}$; (0, I,…IV) – stage indices; (+) – drive side; and (–) – coast side.

As stated in Section 2, it is often assumed that $\Gamma_D(\theta,\dot{\theta}) \approx \Gamma_Q(\theta,\dot{\theta})$ when predicting dynamic responses. Therefore, the chief objective of this article is to essentially address the following question: How does $\Gamma_D(\theta,\dot{\theta})$ relate to $\Gamma_Q(\theta,\dot{\theta})$? More specific questions (as sub-objectives) are posed as follows: (a) Does $\Phi_D(\theta,\dot{\theta}) \approx \Phi_Q(\theta)$ per assumptions made in prior work [12–21]? (b) Does $\Psi_Q(\theta,\dot{\theta})$ fully account for dissipation under dynamic loading? (c) What dissipative mechanism (viscous damping or Coulomb friction) best describes $\Psi_D(\theta,\dot{\theta})$? (d) Given a dynamic response in which the mean operating point rapidly crosses multiple stages, can $\Psi_D(\theta,\dot{\theta})$ be described in a global manner (as assumed in prior work [12,14–16,21]), or must it be described locally (i.e. stage-dependent)? Answers to these questions require experimental and analytical investigation of a multi-staged device, but the scope of analysis is limited to time domain and single degree of freedom nonlinear models. For the sake of simplification, all multi-staged features shall be piecewise linear. Time domain methods of characterizing elastic and dissipative parameters under step responses form the basis of this article.

4. Characterization under quasi-static loading

Characterization under quasi-static loading is typically carried out using a commercial test machine [22,23] (denoted *X–Q*), as conceptually illustrated in Fig. 2a and described by (Eq. (1) and 2). The device is fixed to ground at one end and a low-rate, ramp-like external torque $T_Q(t)$ is slowly applied at the other end. The test machine is instrumented to measure $\theta(t)$ and $\Gamma_Q(t)$ only; therefore, $\theta(t)$ is considered to be the (motion) excitation source, though it is assumed from Eq. (1) that $T_Q(t) \approx \Gamma_Q(t)$. Angular velocity $\dot{\theta}(t)$ is estimated in this paper by applying a forward differencing method to $\theta(t)$, then smoothened using a moving average method [25]. For example, consider a four-staged asymmetric clutch damper (single-disk configuration) with a shaft spline clearance (denoted by subscript 0), drive side ($\theta > 0$, denoted by subscript $+$) and coast side ($\theta < 0$, denoted by subscript $-$). Typical (normalized) measurements are given in Fig. 4; here, time is normalized by $\tau_s \approx 0.1$s (approximately the first natural period of a vehicle powertrain torsional mode [24]), angular displacement is normalized by $\theta_s = \max(|\Theta_{j\pm}|)$, and torque is normalized by $\Gamma_s = \max(|\Gamma_Q(\theta,\dot{\theta})|)$. Measured $\Gamma_Q(\theta,\dot{\theta})$ clearly exhibits path dependence; path P1 begins at $\theta = 0$ and ends at $\theta = \Theta_{\mathrm{IV}+}$ with $\dot{\theta} > 0$; path P2 begins at $\theta = \Theta_{\mathrm{IV}+}$ and ends at $\theta = \Theta_{\mathrm{IV}-}$ with $\dot{\theta} < 0$; and path P3 begins at $\theta = \Theta_{\mathrm{IV}-}$ and ends at $\theta = 0$ with $\dot{\theta} > 0$. Paths P1 and P3 are referred to as the upper paths and P2 as the lower path.

It is assumed that $\Phi_Q(\theta)$ is piecewise linear in nature and can be described by the following equation where $\Phi_{Qj\pm}$ is the median point between the upper and lower paths at $\theta = \Theta_{j\pm}$, $k_{j\pm}$ is the torsional stiffness of each stage, $\Xi(\theta)$ is the unit step function, and N is the total number of stages:

$$\Phi_Q(\theta) = \sum_{j=1}^{N} \left\{ \begin{array}{l} \left[\Phi_{Q(j-\mathrm{I})+} + k_{j+}\left(\theta - \Theta_{(j-\mathrm{I})+}\right)\right]\left[\Xi\left(\theta - \Theta_{(j-\mathrm{I})+}\right) - \Xi\left(\theta - \Theta_{j+}\right)\right] + \ldots \\ \left[\Phi_{Q(j-\mathrm{I})-} + k_{j-}\left(\theta - \Theta_{(j-\mathrm{I})-}\right)\right]\left[\Xi(\theta - \Theta_{\mathrm{I}-}) - \Xi\left(\theta - \Theta_{(j-\mathrm{I})-}\right)\right] \end{array} \right\}, \tag{5}$$

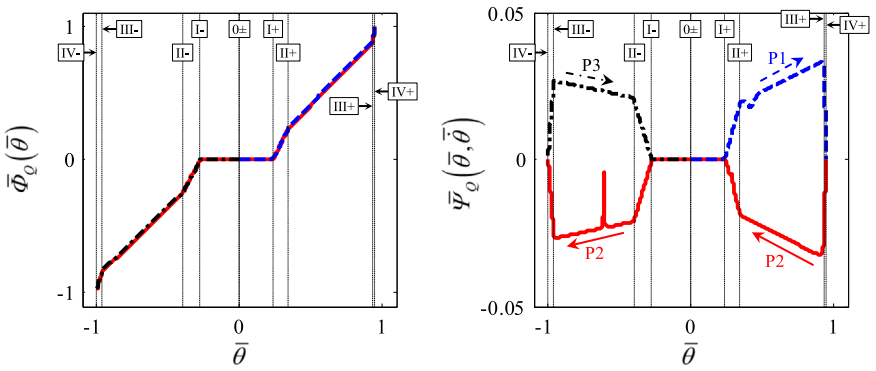

Fig. 5. Predicted elastic and dissipative torques in quasi-static experiment X-Q where $\overline{\Phi}_Q(\bar{\theta})$ is the normalized elastic torque and $\overline{\Psi}_Q(\bar{\theta},\dot{\bar{\theta}})$ is the normalized dissipative torque. Key: (▬ ▬) – path P1; (▬) – path P2; (▪ • ▪) – path P3; (– • –) – angular stage transitions $\Theta_{j\pm}$; (0, I,…IV) – stage indices; (+) – drive side; and (–) – coast side.

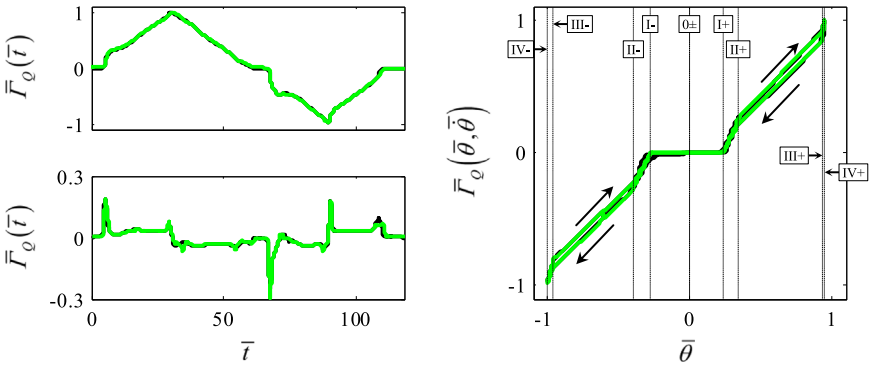

Fig. 6. Predicted and measured (normalized) torque transmission $\overline{\Gamma}_Q$ for quasi-static experiment X-Q, where $\overline{\dot{\Gamma}}_Q$ is the time derivative of $\overline{\Gamma}_Q$. Key: (▪▪) – measurement; (▬) – prediction; (– • –) – angular stage transitions $\Theta_{j\pm}$; (0, I,…IV) – stage indices; (+) – drive side; and (–) – coast side.

$$k_{j+}=\frac{\Phi_{Qj+}-\Phi_{Q(j-1)+}}{\Theta_{j+}-\Theta_{(j-1)+}},\quad k_{j-}=\frac{\Phi_{Q(j-1)-}-\Phi_{Qj-}}{\Theta_{(j-1)-}-\Theta_{j-}}\quad \text{for}\quad j=I,\ \text{II}\ldots N. \tag{6}$$

Since stage $j=0$ is a clearance, $\Phi_Q(\theta)=0$ for $\theta\in[\Theta_{0-}\,\Theta_{0+}]$ and $k_{0\pm}=0$. Dissipative torque $\Psi_Q(\theta,\dot{\theta})$ is described by a multi-staged Coulomb friction element of the following form where $h_Q(\theta)$ is the friction amplitude and η is a regularizing factor [16]

$$\Psi_Q(\theta,\dot{\theta})=h_Q(\theta)\tanh(\eta\dot{\theta}). \tag{7}$$

The friction amplitude $h_Q(\theta)$ is assumed to be piecewise linear and described by the following where $h_{Qj\pm}$ is one half of the difference between the upper and lower paths at $\theta=\Theta_{j\pm}$ and $\Delta h_{Qj\pm}$ is the change in friction amplitude within stage $j\pm$

$$h_Q(\theta)=\sum_{j=1}^{N}\left\{\begin{array}{c}\left[h_{Q(j-1)+}+\Delta h_{Qj+}\left(\theta-\Theta_{(j-1)+}\right)\right]\left[\Xi\left(\theta-\Theta_{(j-1)+}\right)-\Xi\left(\theta-\Theta_{j+}\right)\right]+\ldots\\ \left[h_{Q(j-1)-}+\Delta h_{Qj-}\left(\theta-\Theta_{(j-1)-}\right)\right]\left[\Xi(\theta-\Theta_{1-})-\Xi\left(\theta-\Theta_{(j-1)-}\right)\right]\end{array}\right\}, \tag{8}$$

$$\Delta h_{Qj+}=\frac{h_{Qj+}-h_{Q(j-1)+}}{\Theta_{j+}-\Theta_{(j-1)+}},\quad \Delta h_{Qj-}=\frac{h_{Q(j-1)-}-h_{Qj-}}{\Theta_{(j-1)-}-\Theta_{j-}}\quad \text{for}\quad j=I,\ \text{II}\ldots N. \tag{9}$$

Similar to $\Phi_Q(\theta)$, $\Psi_Q(\theta,\dot{\theta})=0$ for $\theta\in[\Theta_{0-}\Theta_{0+}]$ and $h_{0\pm}=0$. For illustrative purposes, physical domain representations of $\Phi_Q(\theta)$ and $\Psi_Q(\theta,\dot{\theta})$ are given in Fig. 5. To validate the static characterization, measured and predicted $\Gamma_Q(t)$ and $\dot{\Gamma}_Q(t)$ are compared in Fig. 6; note that $\dot{\Gamma}_Q(t)$ is estimated here through numerical differentiation. There is close agreement between the measured and predicted signals as indicated by the mean and maximum (absolute) deviations which are: 0.008 and 0.05, respectively, for $\overline{\Gamma}_Q(\bar{t})$; 0.005 and 0.05, respectively, for $\overline{\dot{\Gamma}}_Q(\bar{t})$.

5. Characterization under dynamic loading

For characterization under dynamic loading, consider the laboratory experiment proposed recently by Krak et al. [21] (denoted X-D), which is conceptually and physically illustrated in Fig. 2b and c and described by (Eqs. (3) and 4). Here, the

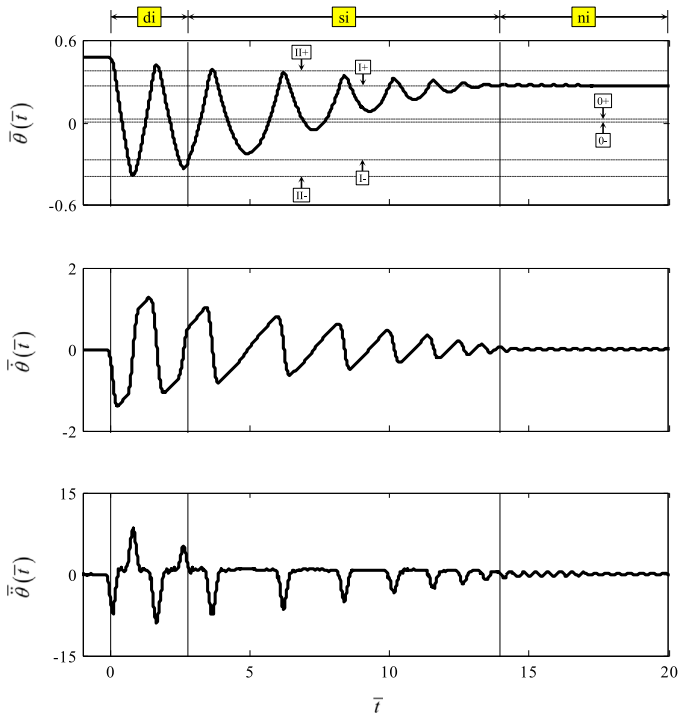

Fig. 7. Typical measured motions from dynamic experiment X-D, where $\overline{\theta}$ is the normalized angular displacement, $\overline{\dot{\theta}}$ is the normalized angular velocity, and $\overline{\ddot{\theta}}$ the is normalized angular acceleration. Key: (▬) – measured motion; (– • –) – angular stage transitions $\Theta_{j\pm}$; (|) – response regime transition; (di, si, ni) – double-sided, single-sided, and no-impact regimes; (0, I, II) – stage indices; (+) – drive side; and (–) – coast side.

device is fixed to ground at one end and has some associated torsional inertia J attached at the other end. A step-like torque $T_D(t)$ is applied to J such that the initial and final operating points of the device $((\theta_o, \Gamma_{Do})$ and $(\theta_f, \Gamma_{Df}))$ lie on separate stages. The experiment is instrumented to measure the translational velocity of a point on J only; then $\theta(t)$, $\dot{\theta}(t)$, and $\ddot{\theta}(t)$ are estimated using system geometry and numerical methods. See Ref. [21] for further details regarding the experiment design, instrumentation, and signal processing. For example, again consider the four-staged asymmetric clutch damper as introduced in Section 1. Measured responses are given in Fig. 7; the normalization follows the same scheme given in Section 4. The responses exhibit richly nonlinear behavior with three distinct response regimes: double-sided impact (di), single-sided impact (si), and no-impact (ni) [21]. These regimes are characterized by significant peak values of $\ddot{\theta}(t)$ which occur at abrupt changes in torsional stiffness, such is found at $\theta = \Theta_{\mathrm{I}\pm}$. Point (θ_o, Γ_{Do}) lies on stage III+ and point (θ_f, Γ_{Df}) lies on stage II+; the path between these points crosses several stages (III− to III+). Note that $\Theta_{0\pm}$ differs between X-D and X-Q experiments due to a variation in assembly.

6. Estimation of elastic parameters

It is problematic to directly estimate $\Gamma_D(\theta, \dot{\theta})$ by substituting measured (estimated) signals $\theta(t)$, $\dot{\theta}(t)$, and $\ddot{\theta}(t)$ into Eq. (4) due to the impulsive and often noisy nature of the measurements. Furthermore, it is difficult to decompose $\Gamma_D(\theta, \dot{\theta})$ into its elastic and dissipative components without a priori knowledge of $\Psi_D(\theta, \dot{\theta})$ and $\Phi_D(\theta, \dot{\theta})$. Therefore, alternative estimation methods must be pursued. For instance, Wallaschek [9] and Rook et al. [26] proposed a stochastic linearization method for estimating effective stiffness parameters of a discontinuous feature under harmonic excitation (stationary process). A similar method is employed here to estimate $\Phi_D(\theta, \dot{\theta})$, though it must be modified to accommodate a non-stationary process, evident from the measured response of X-D. Assume that over a small time window of period τ_g centered at time t the following approximation can be made $\Gamma_D(t) \approx \hat{\Gamma}_D(t)$. Here, $\hat{\Gamma}_D(t)$ is the time history of a linear function as defined below where $\hat{\gamma}_{Dm}(t)$ is the time history of a mean coefficient, $\hat{\gamma}_{Da}(t)$ is the time history of an alternating coefficient, and $\langle \theta, t \rangle_t$ is an instantaneous expected value operator (windowed time average):

$$\hat{\Gamma}_D(t) = \hat{\gamma}_{Dm}(t)\langle \theta, t \rangle_t + \hat{\gamma}_{Da}(t)[\theta(t) - \langle \theta, t \rangle_t]. \tag{10}$$

The instantaneous expected value operator $\langle \theta, t \rangle_t$ is defined by the following where $g(t' - t)$ is a sliding rectangular window of period τ_g, t' is a dummy time variable, t_o is the initial time of the measured response, and t_f is the final time of

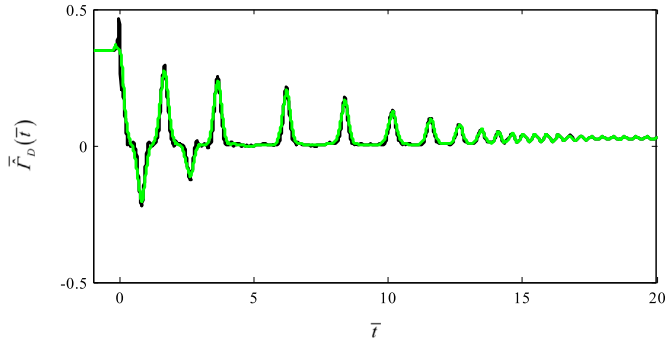

Fig. 8. Effect of window length on the estimated dynamic torque transmission $\bar{\hat{\Gamma}}_D(\bar{t})$ for dynamic experiment X-D in time domain. Key: (▬) $-\tau_g = 0.05\tau_s$; and (▬) $-\tau_g = 0.4\tau_s$.

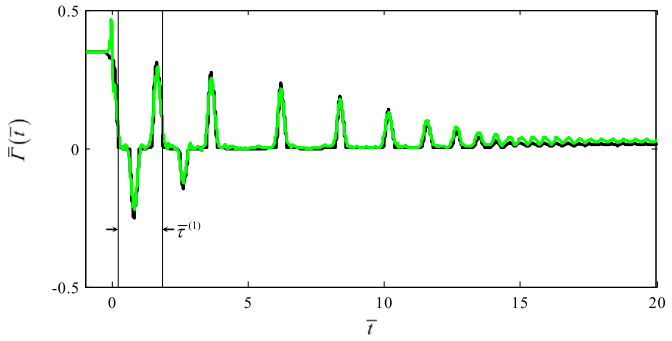

Fig. 9. Comparison of quasi-static $\bar{\Gamma}_Q(\bar{t})$ and estimated dynamic $\bar{\hat{\Gamma}}_D(\bar{t})$torques for dynamic experiment X-D in time domain. Key: (▬) $-\bar{\Gamma}_Q(t)$; (▬) $-\bar{\hat{\Gamma}}_D(t)$; and (|) – limits of period $\bar{\tau}^{(1)}$.

the measured response

$$\langle \theta, t \rangle_t = \frac{\int_{t_o}^{t_f} \theta(t') g(t'-t) \mathrm{d}t'}{\int_{t_o}^{t_f} g(t'-t) \mathrm{d}t'}, \tag{11}$$

$$g(t'-t) = \Xi(t'-t+0.5\tau_g) - \Xi(t'-t-0.5\tau_g). \tag{12}$$

The time histories $\hat{\gamma}_{Dm}(t)$ and $\hat{\gamma}_{Da}(t)$ are treated as time-invariant at time t and thus the following property is assumed:

$$\langle \hat{\gamma}_{Dm}(t), t \rangle_t = \hat{\gamma}_{Dm}(t), \quad \langle \hat{\gamma}_{Da}(t), t \rangle_t = \hat{\gamma}_{Da}(t). \tag{13}$$

Next, $\hat{\Gamma}_D(t)$ is substituted into Eq. (4) to define the following error signal $e(t)$ where $A(t) = T_D(t) - J\ddot{\theta}(t)$

$$e(t) = A(t) - \hat{\Gamma}_D(t). \tag{14}$$

Then, $\langle e^2(t), t \rangle_t$ is minimized with respect to $\hat{\gamma}_{Dm}(t)$ and $\hat{\gamma}_{Da}(t)$ at every time t as follows:

$$\frac{\partial \langle e^2(t), t \rangle_t}{\partial \hat{\gamma}_{Dm}(t)} = 0, \quad \frac{\partial \langle e^2(t), t \rangle_t}{\partial \hat{\gamma}_{Da}(t)} = 0, \tag{15}$$

$$\hat{\gamma}_{Dm}(t) = \frac{\langle A, t \rangle_t \langle \theta, t \rangle_t}{\langle \theta, t \rangle_t^2}, \tag{16}$$

$$\hat{\gamma}_{Da}(t) = \frac{\langle A\theta, t \rangle_t - \langle A, t \rangle_t \langle \theta, t \rangle_t}{\langle \theta^2, t \rangle_t - \langle \theta, t \rangle_t^2}. \tag{17}$$

Calculation of $\hat{\Gamma}_D(t)$ is highly dependent on the duration of τ_g; the approximation becomes local as $\tau_g \to 0$ and global as $\tau_g \to \infty$. To demonstrate this, $\hat{\Gamma}_D(t)$ is calculated for $\tau_g = 0.05\tau_s$ and $\tau_g = 0.4\tau_s$, and displayed in Fig. 8; it is obvious that $\hat{\Gamma}_D(t)$ is smoothened as τ_g increases. Therefore, for this analysis, $\tau_g = 0.05\tau_s$ is selected while recognizing that the duration of τ_g must lie between the sampling period (roughly $0.007\tau_s$) and total length of the measured response (about $20\tau_s$).

For the sake of comparison, $\Gamma_Q(t)$ is calculated using the measured $\theta(t)$ and $\dot{\theta}(t)$ from X-D; the time domain representation is shown in Fig. 9. Observe a close agreement between the two as the mean and maximum absolute differences

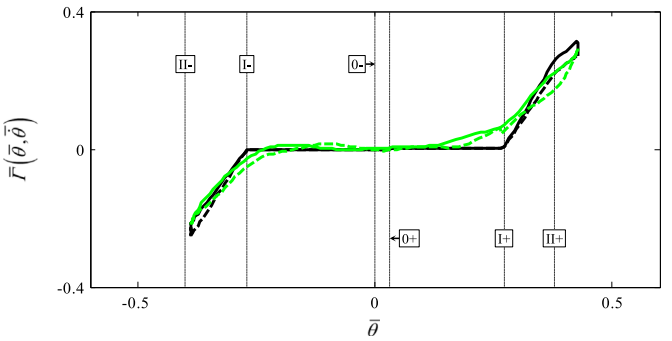

Fig. 10. Comparison of quasi-static $\bar{\Gamma}_Q(\bar{\theta},\dot{\bar{\theta}})$ and estimated dynamic $\bar{\hat{\Gamma}}_D(\bar{\theta},\dot{\bar{\theta}})$ torque for experiment X-D in physical domain over the oscillatory period $\bar{\tau}^{(1)}$. Key: (▬ ▬) $-\bar{\Gamma}_Q(\theta,\dot{\theta}>0)$; (▬ ▬) $-\bar{\Gamma}_Q(\theta,\dot{\theta}<0)$; (▬▬) $-\bar{\hat{\Gamma}}_D(\theta,\dot{\theta}>0)$; (▬ ▬) $-\bar{\hat{\Gamma}}_D(\theta,\dot{\theta}<0)$; (− • −) – angular stage transitions $\Theta_{j\pm}$; (0, I, II) – stage indices; (+) – drive side; and (−) – coast side.

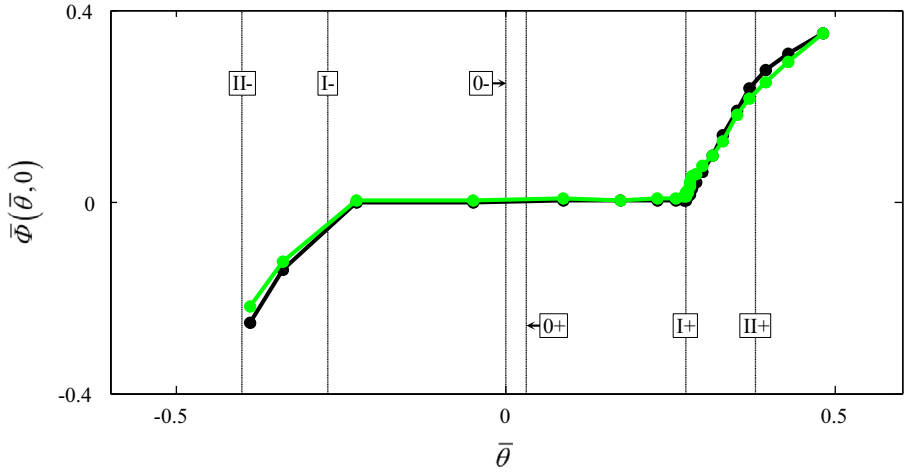

Fig. 11. Comparison of quasi-static elastic $\bar{\Phi}_Q(\bar{\theta})$ and dynamic $\bar{\Phi}_D(\bar{\theta},0)$ elastic torques for experiment X-D in physical domain at $\dot{\theta}=0$. Key: (▬●▬) – $\bar{\Phi}_Q(\bar{\theta})$; (▬●▬) – $\bar{\Phi}_D(\bar{\theta},0)$; (− • −) – angular stage transitions $\Theta_{j\pm}$; (0, I, II) – stage indices; (+) – drive side; and (−) – coast side.

between $\bar{\Gamma}_Q(\bar{t})$ and $\bar{\hat{\Gamma}}_D(\bar{t})$ are 0.02 and 0.10 respectively. The physical domain representation over the first oscillatory period $\tau^{(1)}$ is displayed in Fig. 10; $\hat{\Gamma}_D(\theta,\dot{\theta})$ exhibits both stage and path dependence similar to $\Gamma_Q(\theta,\dot{\theta})$. However, the stage transitions are heavily smoothened during high angular velocity. This is attributed to: (i) a limited sampling period, which is inherent in any measured signal; (ii) the finite window length used by the approximation; and (iii) the fact the linearization approximates the sum of elastic and dissipative torques. Despite this, it is possible to extract some physical insight about $\Phi_D(\theta,\dot{\theta})$. As stated in Section 3, it is assumed that all dissipation ($\Psi_Q(\theta,\dot{\theta})$ and $\Psi_D(\theta,\dot{\theta})$) can be described by viscous damping and/or Coulomb friction, and therefore $\Gamma_Q(\theta,0)=\Phi_Q(\theta)$ and $\Gamma_D(\theta,0)=\Phi_D(\theta,0)$. Accordingly, $\Phi_D(\theta,0)\approx\hat{\Gamma}_D(\theta,0)$, which allows $\Phi_D(\theta,\dot{\theta})$ to be compared to $\Phi_Q(\theta)$ at $\dot{\theta}=0$, as shown in Fig. 11. The first observation is that $\Phi_D(\theta,0)$ and $\Phi_Q(\theta)$ exhibit stage transitions and amplitudes. The mean and maximum absolute differences between $\bar{\Phi}_D(\bar{\theta},0)$ and $\bar{\Phi}_Q(\bar{\theta})$ are roughly 0.02 and 0.05 respectively. Second, $\Phi_D(\theta,0)$ is not strictly piecewise linear, which is most clearly seen at stage II+ (pre-load feature); nevertheless, the absolute difference between $\bar{\Phi}_Q(\bar{\theta})$ and $\bar{\Phi}_D(\bar{\theta},0)$ in stage II+ is at most 0.03. The close agreement between $\Phi_Q(\theta)$ and $\Phi_D(\theta,0)$ supports the assumption made in prior work [12–21] that $\Phi_D(\theta,\dot{\theta})\approx\Phi_Q(\theta)$; this will be further verified by numerical simulation presented in Section 8.

7. Estimation of dissipation parameters

Seven dissipation formulations, which are conceptually illustrated in Fig. 12 and summarized in Table 1, are considered for $\Psi_D(\theta,\dot{\theta})$. It is assumed that one or more of the proposed formulations can effectively describe all dissipative elements within the device. Formulation D0 simply assumes that $\Psi_D(\theta,\dot{\theta})=\Psi_Q(\theta,\dot{\theta})$, which is consistent with literature [12–21]. Formulations D1.1–2 assume global damping, where D1.1 is a single-staged torsional viscous damper c_{D1}, and D1.2 is a single-staged Coulomb element h_{D1}. To facilitate the estimation of parameters, the dissipated energy E_{D1} is defined in terms of both the energy balance principle and dissipation formulations, as given by the following expressions where t_o and t_f are

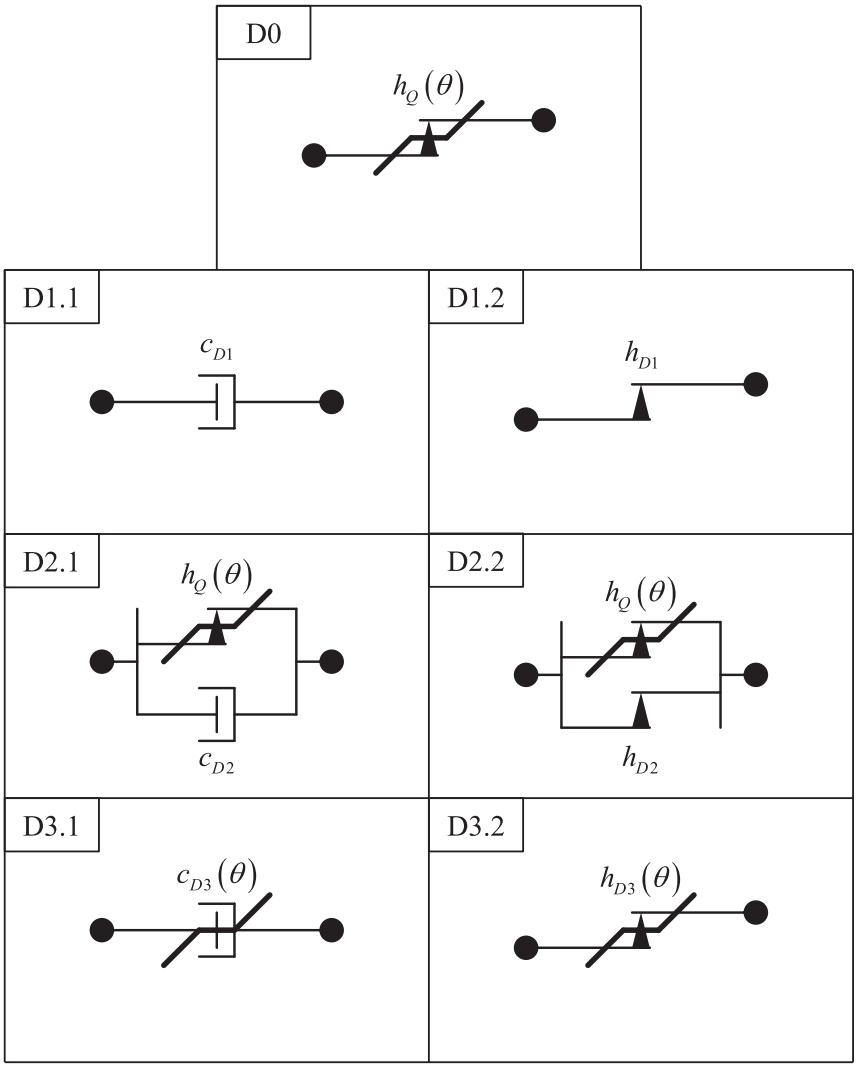

Fig. 12. Conceptual illustration of formulations D0-D3 for the dissipative torque $\Psi_D(\theta,\dot{\theta})$ where θ is the angular displacement, c denotes torsional viscous damping, and h denotes Coulomb friction amplitude.

Table 1
Summary of proposed formulations for dissipative torque $\Psi_D(\theta,\dot{\theta})$ corresponding to Fig. 11.

Model	$\Psi_D(\theta,\dot{\theta})$	Description
D0	$h_Q(\theta)\tanh(\eta\dot{\theta})$	Local (stage-dependent) damping
D1.1	$c_{D1}\dot{\theta}$	Global damping
D1.2	$h_{D1}\tanh(\eta\dot{\theta})$	
D2.1	$h_Q(\theta)\tanh(\eta\dot{\theta})+c_{D2}\dot{\theta}$	Global and local (stage-dependent) damping
D2.2	$[h_Q(\theta)+h_{D2}]\tanh(\eta\dot{\theta})$	
D3.1	$c_{D3}(\theta)\dot{\theta}$	Local (stage-dependent) damping
D3.2	$h_{D3}(\theta)\tanh(\eta\dot{\theta})$	

the initial and final times of the measured response (X-D), W is the external work, ΔU is the change in potential energy, and ΔV is the change in kinetic energy:

$$E_{D1} = W - \Delta U - \Delta V, \tag{18}$$

$$E_{D1} = \int_{t_o}^{t_f} c_{D1}\dot{\theta}^2\,\mathrm{d}t, \quad E_{D1} = \int_{t_o}^{t_f} h_{D1}\tanh(\eta\dot{\theta})\dot{\theta}\,\mathrm{d}t, \tag{19}$$

$$W = \int_{t_o}^{t_f} T_D(t)\dot{\theta}\,\mathrm{d}t, \tag{20}$$

$$\Delta U = \int_{t_o}^{t_f} \Phi_D(\theta,\dot{\theta})\dot{\theta}\,\mathrm{d}t, \tag{21}$$

$$\Delta V = 0.5J\left[\dot{\theta}^2(t_f) - \dot{\theta}^2(t_o)\right]. \tag{22}$$

In Eq. (19), dissipated energy E_{D1} is defined by a time-integral of the dissipative power associated with each formulation (D1.1 and D1.2). This is equivalent to the path-integral of the dissipative torque; however, the time-integral is chosen for the sake of convenience (here and for other dissipative formulations). Next, dissipative parameters c_{D1} and h_{D1} are defined by the following:

$$c_{D1} = E_{D1}\left[\int_{t_o}^{t_f} \dot{\theta}^2\,\mathrm{d}t\right]^{-1}, \tag{23}$$

$$h_{D1} = E_{D1}\left[\int_{t_o}^{t_f} \dot{\theta}\tanh(\eta\dot{\theta})\mathrm{d}t\right]^{-1}. \tag{24}$$

In contrast to D1.1-2, formulations D2.1-2 assume that $\Psi_Q(\theta,\dot{\theta})$ is valid under dynamic loading, though insufficient to completely describe the dissipation. It is assumed here that the residual dissipated energy can be attributed to a global damping element, such as a single-staged torsional viscous damper c_{D2} for formulation D2.1 (consistent with assumptions from prior work [12,14–16,21]) or a single-staged Coulomb element h_{D2} for formulation D2.2. Thus, D2.1-2 is considered a combination of local and global damping elements. To estimate c_{D2} and h_{D2}, an energy balance is again applied to the measured responses of X-D as defined below where W, ΔU, and ΔV are given by (Eqs. (20)–22) and E_{D2} is the dissipated energy:

$$E_{D2} = W - \Delta U - \Delta V, \tag{25}$$

$$E_{D2} = \int_{t_o}^{t_f} \left[c_{D2}\dot{\theta} + \Psi_Q(\theta,\dot{\theta})\right]\dot{\theta}\,\mathrm{d}t, \quad E_{D2} = \int_{t_o}^{t_f} \left[h_{D2}\tanh(\eta\dot{\theta}) + \Psi_Q(\theta,\dot{\theta})\right]\dot{\theta}\,\mathrm{d}t. \tag{26}$$

Dissipative parameters c_{D2} and h_{D2} are then defined by the following:

$$c_{D2} = \left[E_{D2} - \int_{t_o}^{t_f} \Psi_Q(\theta,\dot{\theta})\dot{\theta}\,\mathrm{d}t\right]\left[\int_{t_o}^{t_f} \dot{\theta}^2\,\mathrm{d}t\right]^{-1}, \tag{27}$$

$$h_{D2} = \left[E_{D2} - \int_{t_o}^{t_f} \Psi_Q(\theta,\dot{\theta})\dot{\theta}\,\mathrm{d}t\right]\left[\int_{t_o}^{t_f} \tanh(\eta\dot{\theta})\dot{\theta}\,\mathrm{d}t\right]^{-1}. \tag{28}$$

Formulations D3.1-2 assume that damping must be described locally, where D3.1 utilizes a multi-staged torsional viscous damper $c_{D3}(\theta)$, and D3.2 employs a multi-staged Coulomb element $h_{D3}(\theta)$. Functions $c_{D3}(\theta)$ and $h_{D3}(\theta)$ are assumed to be piecewise linear as given below:

$$c_{D3}(\theta) = \sum_{j=1}^{N} \left\{ \begin{array}{c} \left[c_{D3(j-1)+} + \Delta c_{D3j+}\left(\theta - \Theta_{(j-1)+}\right)\right]\left[\Xi\left(\theta - \Theta_{(j-1)+}\right) - \Xi\left(\theta - \Theta_{j+}\right)\right] + \ldots \\ \left[c_{D3(j-1)-} + \Delta c_{D3j-}\left(\theta - \Theta_{(j-1)-}\right)\right]\left[\Xi\left(\theta - \Theta_{j-}\right) - \Xi\left(\theta - \Theta_{(j-1)-}\right)\right] \end{array} \right\}, \tag{29}$$

$$\Delta c_{D3j+} = \frac{c_{D3j+} - c_{D3(j-1)+}}{\Theta_{j+} - \Theta_{(j-1)+}}, \quad \Delta c_{D3j-} = \frac{c_{D3(j-1)-} - c_{D3j-}}{\Theta_{(j-1)-} - \Theta_{j-}} \quad \text{for} \quad j = I, \text{II} \ldots N, \tag{30}$$

$$h_{D3}(\theta) = \sum_{j=1}^{N} \left\{ \begin{array}{c} \left[h_{D3(j-1)+} + \Delta h_{D3j+}\left(\theta - \Theta_{(j-1)+}\right)\right]\left[\Xi\left(\theta - \Theta_{(j-1)+}\right) - \Xi\left(\theta - \Theta_{j+}\right)\right] + \ldots \\ \left[h_{D3(j-1)-} + \Delta h_{D3j-}\left(\theta - \Theta_{(j-1)-}\right)\right]\left[\Xi\left(\theta - \Theta_{j-}\right) - \Xi\left(\theta - \Theta_{(j-1)-}\right)\right] \end{array} \right\}, \tag{31}$$

$$\Delta h_{D3j+} = \frac{h_{D3j+} - h_{D3(j-1)+}}{\Theta_{j+} - \Theta_{(j-1)+}}, \quad \Delta h_{D3j-} = \frac{h_{D3(j-1)-} - h_{D3j-}}{\Theta_{(j-1)-} - \Theta_{j-}} \quad \text{for} \quad j = I, \text{II} \ldots N. \tag{32}$$

Parameter estimation first requires the definition of dissipative power $\dot{E}_{D3}(t)$ that is

$$\dot{E}_{D3}(t) = T_D(t)\dot{\theta} - \Phi_D(\theta,\dot{\theta})\dot{\theta} - J\ddot{\theta}\dot{\theta}. \tag{33}$$

Next, the energy dissipated in each stage $E_{D3j\pm}$ is calculated using the following:

$$E_{D3j+} = \int_{t_o}^{t_f} \dot{E}_{D3}(t)\left[\Xi\left(\theta - \Theta_{(j-1)+}\right) - \Xi\left(\theta - \Theta_{j+}\right)\right]\mathrm{d}t, \tag{34}$$

Table 2
Intermediate parameters used in the estimation of $c_{D3j\pm}$ and $h_{D3j\pm}$ for dissipative formulation D3.1-2.

Intermediate parameter	Definition
α_{cj+}	$\int_{t_o}^{t_f} \dot{\theta}^2 [\Xi(\theta-\Theta_{(j-1)+}) - \Xi(\theta-\Theta_{j+})]\,dt$
α_{cj-}	$\int_{t_o}^{t_f} \dot{\theta}^2 [\Xi(\theta-\Theta_{j-}) - \Xi(\theta-\Theta_{(j-1)-})]\,dt$
β_{cj+}	$\int_{t_o}^{t_f} \dot{\theta}^2 \left(\frac{\theta-\Theta_{(j-1)+}}{\Theta_{j+}-\Theta_{(j-1)+}}\right) [\Xi(\theta-\Theta_{(j-1)+}) - \Xi(\theta-\Theta_{j+})]\,dt$
β_{cj-}	$\int_{t_o}^{t_f} \dot{\theta}^2 \left(\frac{\theta-\Theta_{(j-1)-}}{\Theta_{(j-1)-}-\Theta_{j-}}\right) [\Xi(\theta-\Theta_{j-}) - \Xi(\theta-\Theta_{(j-1)-})]\,dt$
α_{hj+}	$\int_{t_o}^{t_f} \tanh(\eta\dot{\theta})\dot{\theta} [\Xi(\theta-\Theta_{(j-1)+}) - \Xi(\theta-\Theta_{j+})]\,dt$
α_{hj-}	$\int_{t_o}^{t_f} \tanh(\eta\dot{\theta})\dot{\theta} [\Xi(\theta-\Theta_{j-}) - \Xi(\theta-\Theta_{(j-1)-})]\,dt$
β_{hj+}	$\int_{t_o}^{t_f} \tanh(\eta\dot{\theta})\dot{\theta} \left(\frac{\theta-\Theta_{(j-1)+}}{\Theta_{j+}-\Theta_{(j-1)+}}\right) [\Xi(\theta-\Theta_{(j-1)+}) - \Xi(\theta-\Theta_{j+})]\,dt$
β_{hj-}	$\int_{t_o}^{t_f} \tanh(\eta\dot{\theta})\dot{\theta} \left(\frac{\theta-\Theta_{(j-1)-}}{\Theta_{(j-1)-}-\Theta_{j-}}\right) [\Xi(\theta-\Theta_{j-}) - \Xi(\theta-\Theta_{(j-1)-})]\,dt$

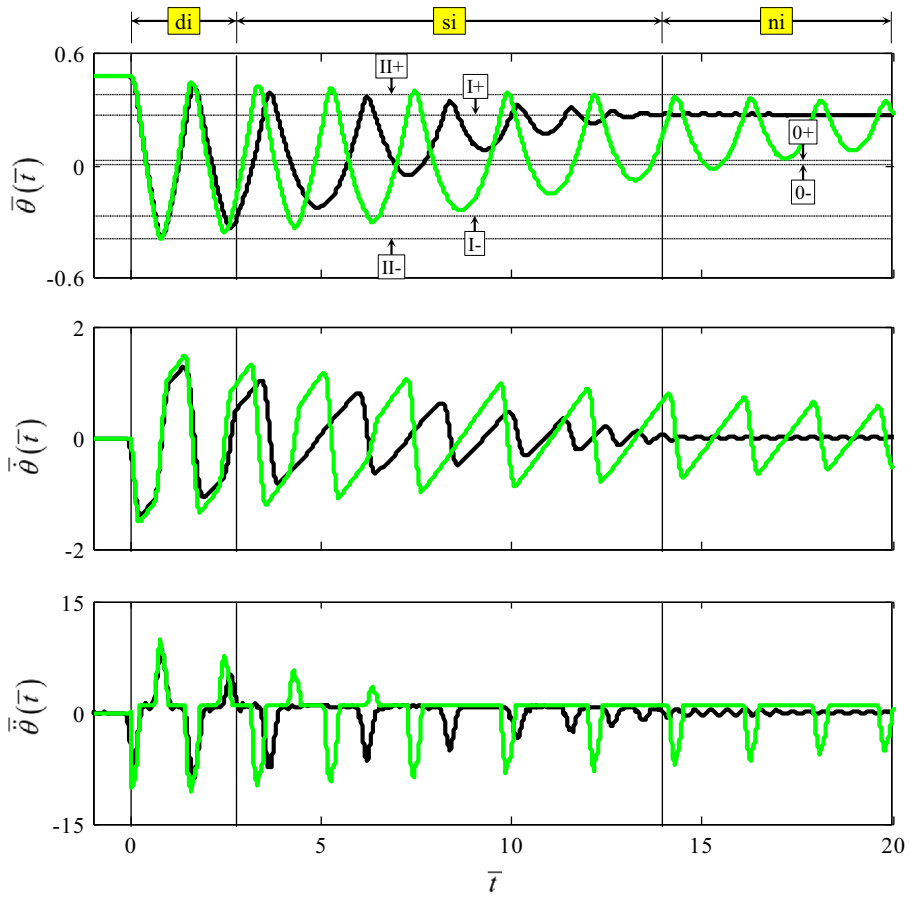

Fig. 13. Comparison between measured and predicted (with formulation D0) motions for experiment X-D. Key: (▬) – measured motion; (▬) – predicted motion; (– • –) – angular stage transitions $\Theta_{j\pm}$; (I) – regime transitions of the measured response; (di, si, ni) – double-sided, single-sided, and no-impact regimes of the measured response; (0, I, II) – stage indices; (+) – drive side; and (–) – coast side.

$$E_{D3j-} = \int_{t_o}^{t_f} \dot{E}_{D3}(t)\left[\Xi(\theta-\Theta_{j-}) - \Xi(\theta-\Theta_{(j-1)-})\right]dt. \tag{35}$$

The energy dissipated in each stage is also defined as follows:

$$E_{D3j+} = \int_{t_o}^{t_f} \left[c_{D3(j-1)+} + \Delta c_{D3j+}(\theta-\Theta_{(j-1)+})\right]\dot{\theta}^2 \left[\Xi(\theta-\Theta_{(j-1)+}) - \Xi(\theta-\Theta_{j+})\right]dt, \tag{36}$$

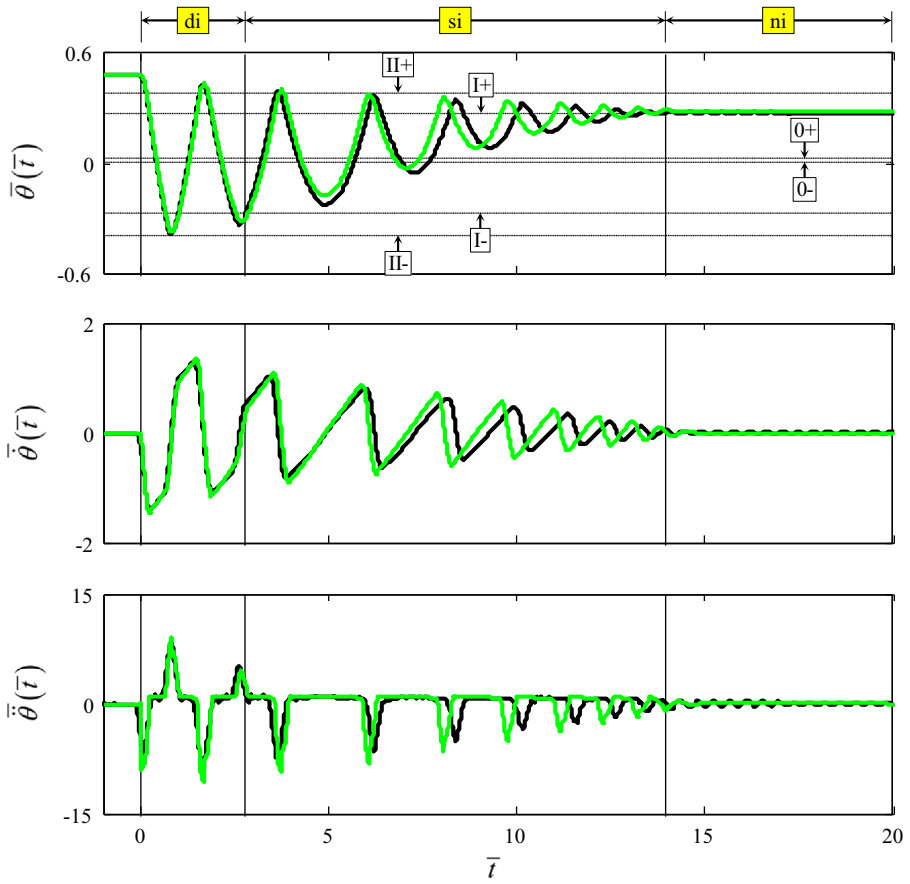

Fig. 14. Comparison between measured and predicted (with formulation D3.2) motions for experiment X-D. Key: (▬ ▬) – measured motion; (▬▬) – predicted motion; (– • –) – angular stage transitions $\Theta_{j\pm}$; (|) – regime transitions of the measured response; (di, si, ni) – double-sided, single-sided, and no-impact regimes of the measured response; (0, I, II) – stage indices; (+) – drive side; and (–) – coast side.

$$E_{D3j+} = \int_{t_o}^{t_f} \left[c_{D3(j-1)+} + \Delta c_{D3j+}\left(\theta - \Theta_{(j-1)+}\right)\right]\dot{\theta}^2\left[\Xi\left(\theta - \Theta_{(j-1)+}\right) - \Xi\left(\theta - \Theta_{j+}\right)\right]\mathrm{d}t, \tag{37}$$

$$E_{D3j+} = \int_{t_o}^{t_f} \left[h_{D3(j-1)+} + \Delta h_{D3j+}\left(\theta - \Theta_{(j-1)+}\right)\right]\tanh(\eta\dot{\theta})\dot{\theta}\left[\Xi\left(\theta - \Theta_{(j-1)+}\right) - \Xi\left(\theta - \Theta_{j+}\right)\right]\mathrm{d}t, \tag{38}$$

$$E_{D3j-} = \int_{t_o}^{t_f} \left[h_{D3(j-1)-} + \Delta h_{D3j-}\left(\theta - \Theta_{(j-1)-}\right)\right]\tanh(\eta\dot{\theta})\dot{\theta}\left[\Xi\left(\theta - \Theta_{j-}\right) - \Xi\left(\theta - \Theta_{(j-1)-}\right)\right]\mathrm{d}t. \tag{39}$$

Parameters $c_{D3j\pm}$ and $h_{D3j\pm}$ are then calculated by combining (Eqs. (34)–39) as given below where it is assumed that $c_{D30\pm} = h_{D30\pm} = 0$, and intermediate parameters $\alpha_{cj\pm}$, $\beta_{cj\pm}$, $\alpha_{hj\pm}$, and $\beta_{hj\pm}$ are defined in Table 2

$$c_{D3j+} = \left[E_{D3j+} + c_{D3(j-1)+}\left(\beta_{cj+} - \alpha_{cj+}\right)\right]\beta_{cj+}^{-1}, \tag{40}$$

$$c_{D3j-} = \left[c_{D3(j-1)-}\left(\alpha_{cj-} - \beta_{cj-}\right) - E_{D3j-}\right]\beta_{cj-}^{-1}, \tag{41}$$

$$h_{D3j+} = \left[E_{D3j+} + h_{D3(j-1)+}\left(\beta_{hj+} - \alpha_{hj+}\right)\right]\beta_{hj+}^{-1}, \tag{42}$$

$$h_{D3j-} = \left[h_{D3(j-1)-}\left(\alpha_{hj-} - \beta_{hj-}\right) - E_{D3j-}\right]\beta_{hj-}^{-1}. \tag{43}$$

8. Comparative assessment of dissipative formulations

To validate the proposed formulations, time domain simulations of the dynamic experiment (X-D) are conducted using a commercial numerical solver [21,25] since it is commonly used in the vehicle industry. Comparisons between measured and predicted motions from formulations D0 and D3.2 are shown in Figs. 13 and 14, respectively; predictions from formulations

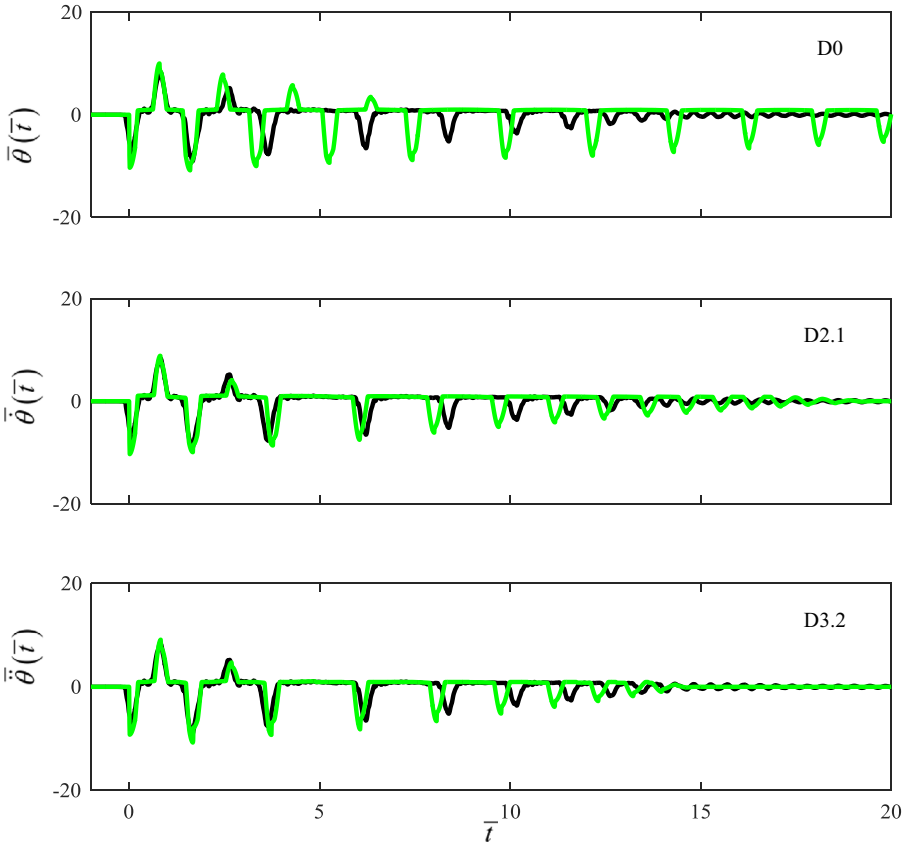

Fig. 15. Comparison between measured and predicted (with formulations D0, D2.1, and D3.2) $\bar{\bar{\theta}}(\bar{t})$ for experiment X-D. Key: (▬) – measurement; and (▬) – prediction.

Table 3
Summary of the response metrics ($R1$–$R6$) for several dissipation formulations (D1–D3): (a–c) normalized geometric norm of error between measurement and prediction; and (d) absolute difference between measured and predicted response regime periods. The ideal value for each metric is 0 (zero) and the worst case is associated with a very high positive value; lowest values ("best") per metric are emboldened.

	D1.1	D1.2	D2.1	D2.2	D3.1	D3.2
(a) Measured double-sided impact regime di						
$R1(\theta)$	**0.18**	0.95	0.28	0.24	1.28	0.38
$R1(\dot{\theta})$	0.30	0.90	0.36	**0.28**	0.98	0.38
$R1(\ddot{\theta})$	0.58	0.92	0.58	**0.51**	1.06	0.56
(b) Measured single-sided impact regime si						
$R2(\theta)$	0.32	0.51	0.31	0.31	0.41	**0.26**
$R2(\dot{\theta})$	0.45	0.67	0.45	0.46	0.50	**0.40**
$R2(\ddot{\theta})$	0.64	0.82	0.64	0.64	0.62	**0.60**
(c) Measured no-impact regime ni						
$R3(\theta)$	0.19	**0.04**	0.10	**0.04**	0.20	**0.04**
$R3(\dot{\theta})$	0.41	**0.04**	0.22	0.05	0.44	**0.04**
$R3(\ddot{\theta})$	0.54	0.11	0.33	0.12	0.58	0.12
(d) Absolute difference between measured and predicted response regime periods						
$R4$ (di)	0.04	1.85	0.07	**0.03**	0.27	0.06
$R5$ (si)	>5.84	2.04	2.84	**0.26**	>5.81	0.27
$R6$ (ni)	N/A	**0.19**	2.91	0.29	N/A	0.21

D1.1-2, D2.1-2, and D3.1 are displayed in Appendix B. Additionally, comparisons between measurements and predictions from formulation D0, D2.1, and D3.2 are shown in Fig. 15. Upon initial observation, it is evident that $\Psi_Q(\theta,\dot{\theta})$ (formulation D0) alone is not sufficient to describe dissipation under dynamic loading and that predictions from D1-3 are superior to D0. Geometric norms of prediction error are defined over each regime (di, si, and ni) of the measured responses as given below

where $\theta(t)$ is the measured signal, $\theta(t, \mathrm{D}a.b)$ is predicted from formulation D$a.b$ (a={1, 2, 3}, b={1, 2}), and $\theta(t, \mathrm{D0})$ is the prediction from formulation D0

$$R1(\theta) = \left(\frac{\int_{t_o}^{t_o+\tau_{\mathrm{di}}} \left[\theta(t) - \theta(t, \mathrm{D}a.b)\right]^2 \mathrm{d}t}{\int_{t_o}^{t_o+\tau_{\mathrm{di}}} \left[\theta(t) - \theta(t, \mathrm{D0})\right]^2 \mathrm{d}t} \right)^{0.5}, \tag{44}$$

$$R2(\theta) = \left(\frac{\int_{t_o+\tau_{\mathrm{di}}}^{t_o+\tau_{\mathrm{di}}+\tau_{\mathrm{si}}} \left[\theta(t) - \theta(t, \mathrm{D}a.b)\right]^2 \mathrm{d}t}{\int_{t_o+\tau_{\mathrm{di}}}^{t_o+\tau_{\mathrm{di}}+\tau_{\mathrm{si}}} \left[\theta(t) - \theta(t, \mathrm{D0})\right]^2 \mathrm{d}t} \right)^{0.5}, \tag{45}$$

$$R3(\theta) = \left(\frac{\int_{t_o+\tau_{\mathrm{di}}+\tau_{\mathrm{si}}}^{t_f} \left[\theta(t) - \theta(t, \mathrm{D}a.b)\right]^2 \mathrm{d}t}{\int_{t_o+\tau_{\mathrm{di}}+\tau_{\mathrm{si}}}^{t_f} \left[\theta(t) - \theta(t, \mathrm{D0})\right]^2 \mathrm{d}t} \right)^{0.5}. \tag{46}$$

For additional metrics, the absolute differences between the normalized measured and predicted response regime periods are defined as

$$R4 = \left| \overline{\tau}_{\mathrm{di}} - \overline{\tau}_{\mathrm{di}}(\mathrm{D}a.b) \right|, \tag{47}$$

$$R5 = \left| \overline{\tau}_{\mathrm{si}} - \overline{\tau}_{\mathrm{si}}(\mathrm{D}a.b) \right|, \tag{48}$$

$$R6 = \left| \overline{\tau}_{\mathrm{ni}} - \overline{\tau}_{\mathrm{ni}}(\mathrm{D}a.b) \right|. \tag{49}$$

The ideal value for each metric is 0 (zero) and the worst case is associated with a very high positive value; thus, "best" metric values are those nearest to 0 (as summarized in Table 3). It is evident (from the metrics, Figs. 13 and 14, and Appendix B) that predictions from dissipative formulations D2.1, D2.2, and D3.2 (see Fig. 12 for illustrations) have the closest agreement to the measurements. These predictions are very similar to the measurement (and each other) in the double (di) and single-sided impact (si) regimes, where the motion spans several stages and the angular velocity is relatively high. However, when the response is confined to a single stage (no-impact regime (ni)), the angular velocity decreases; now, the prediction from D2.1 (which is the formulation most similar to prior work [12–16,19–21]) is significantly worse than those from D2.2 and D3.2 (current work). This can clearly be seen in Fig. 15. The reduced accuracy of D2.1 could be explained by the following: (1) As angular velocity decreases, the effect of viscous damping also decreases, unlike a Coulomb friction element; and (2) The stage-dependent element in D2.1 is estimated under quasi-static loading only. The predictions from D2.2 and D3.2 are too similar to declare that one is more accurate than the other. Nevertheless, these results suggest that over wide ranges of angular displacement (across several stages) and velocity, the effective dissipative formulation of the device is best described by a pure Coulomb friction element (unlike formulation D2.1 and prior work [12–16,19–21]) that incorporates stage-dependence, such as formulations D2.2 and D3.2. Additionally, both quasi-static and dynamic experiments must be utilized to accurately estimate all parameters (e.g. angular stage transitions Θ, Coulomb friction amplitude h, and regularizing factor η).

9. Conclusion

The main contribution of this article is the development of a new time domain parameter estimation method for a practical torsional device (such as a vehicle clutch damper) with multiple discontinuous nonlinearities that subject to dynamic, transient loading. Under current engineering practice [11–23], vehicle clutch dampers are usually characterized from a quasi-static experiment only and linear viscous damping parameters are assumed. The proposed method compares characterization of the device under quasi-static and dynamic loading conditions, which addresses a critical need in both industrial practice and scientific literature. Following the suggestions of Kerschen et al. [1], the proposed method utilizes measurements collected from a component-level dynamic experiment, which offers the following intrinsic advantages: (1) the interaction between multiple nonlinear features is maintained; (2) experimentation conditions could be more similar to the operating environment; and (3) fewer measurements from laboratory experiments are required.

An instantaneous stochastic linearization technique is first proposed to estimate and verify the underlying elastic parameters. Dissipative parameters are estimated using the energy balance principle and a model-based approach (with seven alternate formulation) through it is limited to single or multi-staged torsional viscous dampers and Coulomb friction elements. Answers to the questions posed (under objectives in Section 3) are summarized as follows: (a) Elastic parameters under quasi-static and dynamic loading are very similar, which is consistent with the assumptions made in literature [12–21]. (b) The multi-staged Coulomb friction estimated under quasi-static loading is insufficient to account for the dissipation under dynamic loading; however, the addition of a parallel single-staged torsional viscous damper or Coulomb friction element improves predictions. (c) Dissipation under dynamic loading is better described by the Coulomb friction rather than torsional viscous damping. (d) When the mean operating point of a dynamic response crosses one or more stages, damping must be described in a local or stage-dependent manner. Given the successful application demonstrated in this study, the proposed method could be extended to the characterization and modeling of similar physical systems with

discontinuous nonlinearities. Finally, this method should be valuable tool for improving the design and dynamic analysis of a family nonlinear isolators and dampers.

Acknowledgment

The authors acknowledge Eaton Corporation (Clutch Division) for supporting this research. We would like to thank Luiz Pereira and Brian Franke for their assistance with experimental studies. Further, we acknowledge the member organizations of the Smart Vehicle Concepts Center (www.SmartVehicleCenter.org) and the National Science Foundation.

Appendix A. List of symbols

Symbols (with dimensional units)

0, *I*, II…	Stage indices	n/a
c	Torsional viscous damping	N m s rad^{-1}
$E, \dot{E}$	Dissipative energy and power	J, J s^{-1}
h	Coulomb hysteresis amplitude	N m
J	Torsional inertia	kg m^2
k	Torsional stiffness	N m rad^{-1}
N	Number of clutch damper stages	n/a
t	Time	s
T	External torque	N m
U	Potential energy	J
V	Kinetic energy	J
W	External work	J
α	Coefficient for parameter estimation	rad or rad^2•s^{-1}
β	Coefficient for parameter estimation	rad or rad^2 s^{-1}
γ	Coefficient for torque transmission approximation	N m rad^{-1}
Γ	Torque transmission	N m
Δ	Finite change	n/a
η	Angular velocity regularizing factor (Coulomb friction)	s rad^{-1}
$\theta, \dot{\theta}, \ddot{\theta}$	Angular displacement, velocity, and acceleration	rad, rad s^{-1}, rad^{-2}
Θ	Angular stage transition	rad
Ξ	Unit-step function	n/a
τ	Period (time)	s
Φ	Elastic torque transmission	N m
Ψ	Dissipative torque transmission	N m
$+$	Drive side	n/a
$-$	Coast side	n/a

Subscripts

0, I, II...	Stage indices
a	Alternating
D	Dynamic loading conditions
di	Double-sided impact regime
f	Final
i – hub	Clutch damper inner hub
j	Stage index
m	Mean
n	Natural
ni	No-impact regime
o	Initial
o – hub	Clutch damper outer hub
Q	Quasi-static loading conditions
s	Scaling factor
si	Single-sided impact regime
t	Instantaneous (time dependent)
ε	Small value approximated by 0
$+$	Drive side
$-$	Coast side

Superscripts

(i)	Oscillatory period index
$\bar{}$	Normalized
$'$	Dummy variable
$\hat{}$	Approximation

Abbreviations

di	Double-sided impact regime
si	Single-sided impact regime
ni	No-impact regime
P1, P2, P3	Paths under quasi-static loading
X-D	Experiment under dynamic loading
X-Q	Experiment under quasi-static loading
D0, D*a.b*	Proposed dissipative formulations for dynamic loading ($a=\{1, 2, 3\}$; $b=\{1, 2\}$)
*R*1…6	Predicted response metrics

Appendix B. Comparative results for other dissipation formulations

See Appendix Figs. B1–B5.

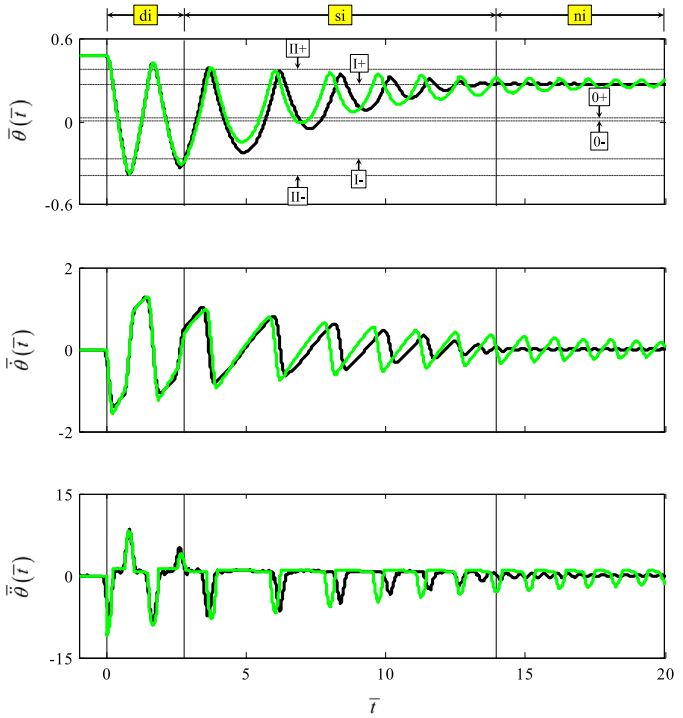

Fig. B1. Comparison between measured and predicted (with formulation D1.1) motions for dynamic experiment X-D, where $\bar{\theta}$ is the normalized angular displacement, $\dot{\bar{\theta}}$ is the normalized angular velocity, and $\ddot{\bar{\theta}}$ is the normalized angular acceleration. Key: (▪▪) – measured motion; (▬) – predicted motion; $(-\bullet-)$ – angular stage transitions $\Theta_{j\pm}$; $(|)$ – regime transitions of the measured response; (di, si, ni) – double-sided, single-sided, and no-impact regimes of the measured response; (0, I, II) – stage indices; $(+)$ – drive side; and $(-)$ – coast side.

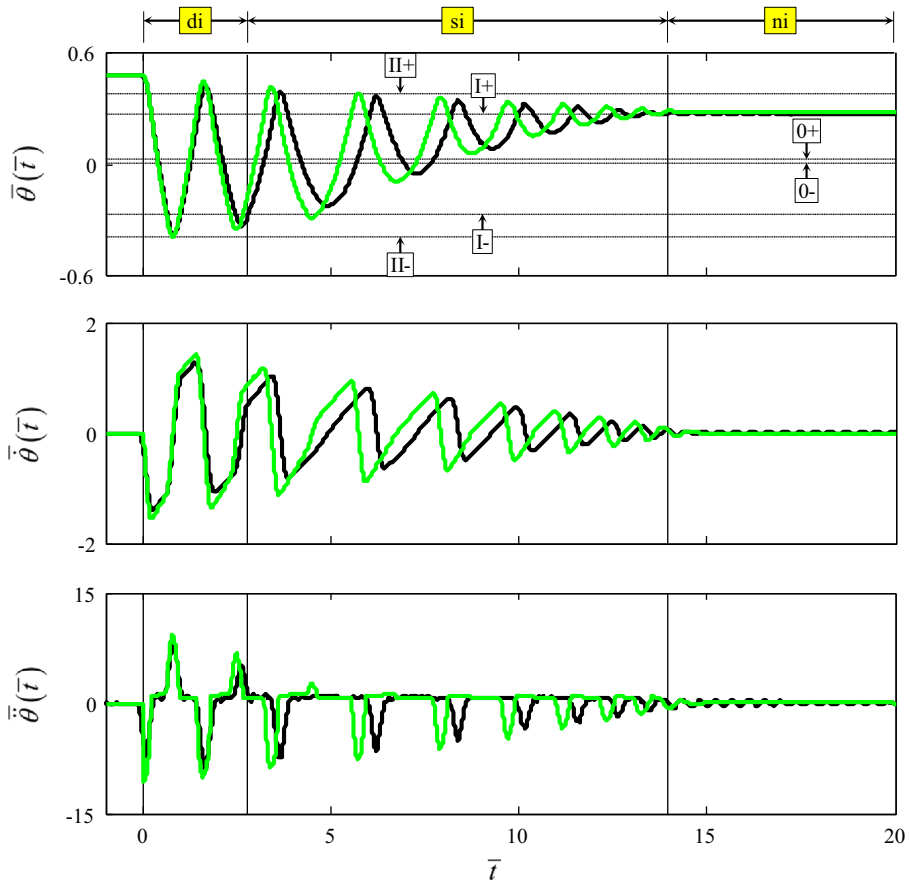

Fig. B2. Comparison between measured and predicted (with formulation D1.2) motions for dynamic experiment X-D. Key is described in Fig. B1 caption.

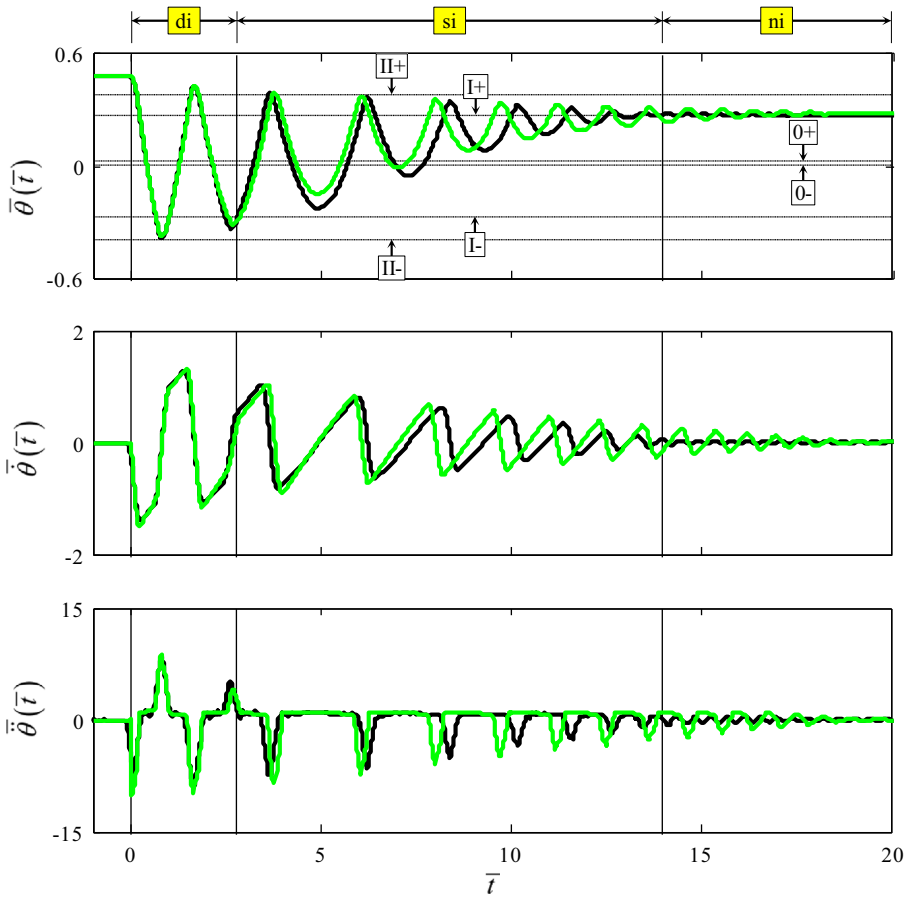

Fig. B3. Comparison between measured and predicted (with formulation D2.1) motions for dynamic experiment X-D. Key is described in Fig. B1 caption.

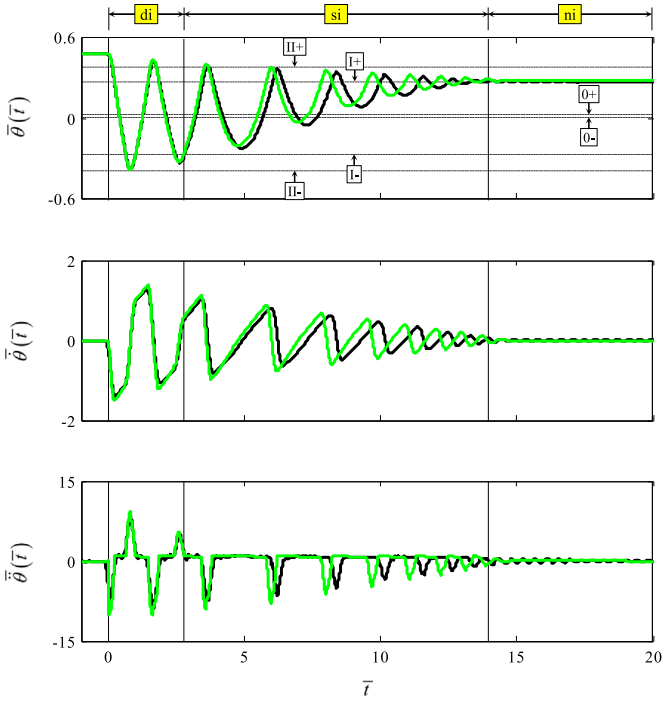

Fig. B4. Comparison between measured and predicted (with formulation D2.2) motions for dynamic experiment X-D. Key is described in Fig. B1 caption.

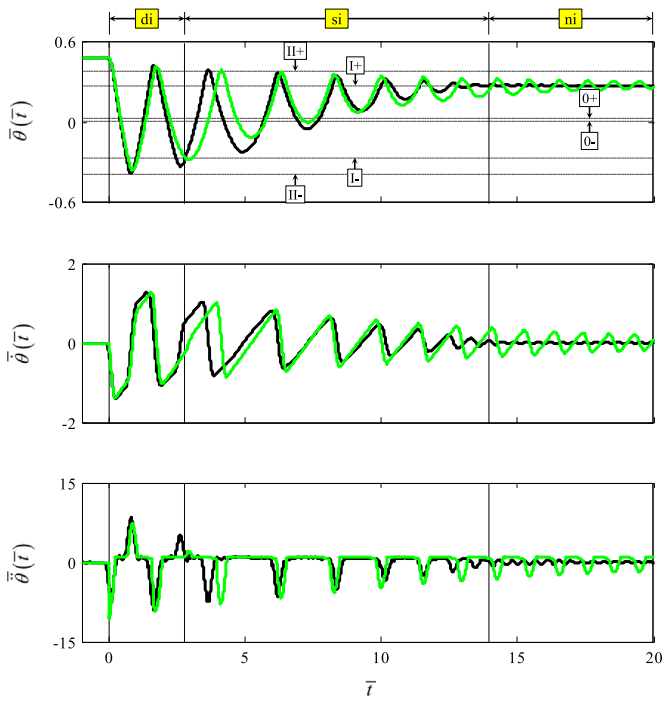

Fig. B5. Comparison between measured and predicted (with formulation D3.1) motions for dynamic experiment X-D. Key is described in Fig. B1 caption.

References

[1] G. Kerschen, K. Worden, A.F. Vakakis, J.C. Golinval, Past, present and future of nonlinear system identification in structural dynamics, *Mechanical Systems and Signal Processing* 20 (2006) 505–592, http://dx.doi.org/10.1016/j.ymssp.2005.04.008.

[2] P. Eret, C. Meskell, A practical approach to parameter identification for a lightly damped, weakly nonlinear system, *Journal of Sound and Vibration* 310 (2008) 829–844, http://dx.doi.org/10.1016/j.jsv.2007.08.002.

[3] B.F. Feeny, J.W. Liang, A decrement method for the simultaneous estimation of Coulomb and viscous friction, *Journal of Sound and Vibration* 195 (1996) 149–154, http://dx.doi.org/10.1006/jsvi.1996.0411.

[4] B.F. Feeny, C.M. Yuan, J.P. Cusumano, Parametric identification of an experimental magneto-elastic oscillator, *Journal of Sound and Vibration* 247 (2001) 785–806, http://dx.doi.org/10.1006/jsvi.2001.3694.

[5] J.W. Liang, B.F. Feeny, Balancing energy to estimate damping in a forced oscillator with compliant contact, *Journal of Sound and Vibration* 330 (2011) 2049–2061, http://dx.doi.org/10.1016/j.jsv.2010.11.015.

[6] V. Lampaert, F. Al-Bender, J. Swevers, Experimental characterization of dry friction at low velocities on a developed tribometer setup for macroscopic measurements, *Tribology Letters* 16 (2004) 95–105, http://dx.doi.org/10.1023/B:TRIL.0000009719.53083.9e.

[7] J. Wojewoda, A. Stefański, M. Wiercigroch, T. Kapitaniak, Hysteretic effects of dry friction: modelling and experimental studies, *Philosophical Transactions of Royal Society* 366 (2008) 747–765, http://dx.doi.org/10.1098/rsta.2007.2125.

[8] J.M. Londoño, S.A. Neild, J.E. Cooper, Identification of backbone curve of nonlinear systems from resonance decay responses, *Journal of Sound and Vibration* 348 (2015) 224–238, http://dx.doi.org/10.1016/j.jsv.2015.03.015.

[9] J. Wallaschek, Dynamics of non-linear automobile shock-absorbers, *International Journal of Non-linear Mechanics* 25 (1990) 299–308, http://dx.doi.org/10.1016/0020-7462(90)90059-I.

[10] R.A. Ibrahim, Recent advances in nonlinear passive vibration isolators, *Journal of Sound and Vibration* 314 (2008) 371–452, http://dx.doi.org/10.1016/j.jsv.2008.01.014.

[11] F. Shaver, *Manual Transmission Clutch Systems*, SAE, 1997.

[12] Ph Couderc, J. Callenaere, J. Der Hagopian, G. Ferraris, A. Kassai, Y. Borjesson, L. Verdillon, S. Gairmard, Vehicle driveline dynamic behavior: experimentation and simulation, *Journal of Sound and Vibration* 218 (1998) 133–157, http://dx.doi.org/10.1006/jsvi.1998.1808.

[13] C.L. Gaillard, R. Singh, Dynamic analysis of automotive clutch dampers, *Applied Acoustics* 60 (2000) 399–424, http://dx.doi.org/10.1016/S003-682X(00)00005-0.

[14] W. Oh, R. Singh, Examination of clunk phenomena using a non-linear torsional model of a front-wheel drive vehicle with manual transmission, *2005 SAE Noise and Vibration Conference*, Traverse City, MI, May 16–19 2005, SAE Paper 2005-01-2291. http://dx.doi.org/10.4271/2005-01-2291.

[15] J.Y. Yoon, R. Singh, Effect of multi-stage clutch damper characteristics on transmission gear rattle under two engine conditions, *ProcIMechE Part D: Journal of Automobile Engineering* 277 (2013) 1273–1295, http://dx.doi.org/10.1177/0954407013493267.

[16] L. Li, R. Singh, Analysis of start-up transient for a powertrain system with a nonlinear clutch damper, *Mechanical Systems and Signal Processing* 62–63 (2015) 460–479, http://dx.doi.org/10.1016/j.ymssp.2015.03.001.

[17] A. Szadkowski, N. Naganathan, TORANTM: A comprehensive simulation tool for driveline torsionals, *SAE Technical Paper 942322*, 1994. doi: 10.4271/942322.

[18] A. Szadkowski, E. Prange, N. Naganathan, Hysteresis effects on driveline torsional vibrations, *SAE Technical Paper 951293*, 1995. doi: 10.4271/951293.

[19] J.W. Biermann, B. Hagerodt, Investigation of the clonk phenomenon in vehicle transmissions – measurement, modelling, and simulation, *Proc. IMechE Part K: Journal of Multi-body Dynamics* 213 (1999) 53–60, http://dx.doi.org/10.1243/1464419991544054.

[20] M.T. Menday, H. Rahnejat, M. Ebrahimi, Clonk: an onomatopoeic response in torsional impact of automotive drivelines, *Proceedings of the Institution of Mechanical Engineers Part D: Journal of Automobile Engineering* 213 (1999) 349–357, http://dx.doi.org/10.1243/0954407991526919.

[21] M.D. Krak, J.T. Dreyer, R. Singh, Development of a non-linear clutch damper experiment exhibiting transient dyanmics, *SAE Int. J. Passeng. Cars – Mech. Syst.* 8 (2015) 754–761, http://dx.doi.org/10.4271/2015-01-2189.

[22] Zwick Roell Group, Clutch testing – axial/torsional, ⟨⟨http://www.zwickusa.com⟩⟩, 2015 (accessed October 2015).

[23] MTS Systems Corporation, Transmission component test benches, ⟨http://www.mts.com⟩, 2015 (accessed October 2015).
[24] A.R. Crowther, R. Singh, N. Zhang, C. Chapman, Impulsive response of an automotive transmission system with multiple clearances: formulation, simulation, and experiment, *Journal of Sound and Vibration* 306 (2007) 444–466, http://dx.doi.org/10.1016/j.jsv.2007.05.053.
[25] MATLAB, MathWorks, ⟨http://www.mathworks.com/products/matlab/⟩, 2015 (accessed October 2015).
[26] T.E. Rook, R. Singh, Dynamic analysis of a reverse-idler gear pair with concurrent clearances, *Journal of Sound and Vibration* 182 (1995) 303–322, http://dx.doi.org/10.1006/jsvi.1994.0198.